Two-dimensional character of an amorphous state in a eutectoid reaction of a Ti–40 at. % Al alloy

M. Tanimura and Y. Inoue
Structural Analysis Section, Research Department, Nissan ARC Ltd., 1, Natsushima-cho, Yokosuka-shi 237, Japan

Y. Koyama
Kagami Memorial Laboratory for Materials Science and Technology and Department of Materials Science and Engineering, Waseda University, Shinjuku-ku, Tokyo 169, Japan

(Received 30 September 1996; revised manuscript received 17 January 1997)

Morphological and crystallographic features of an amorphous state appearing in an initial stage of a eutectoid reaction in a Ti–40 at. % Al alloy have been investigated by transmission electron microscopy. Dark field images with different electron incidences, which were taken by using a part of a halo ring, indicate that the shape of the amorphous-state region is basically a plate, the normal of which is parallel to the $[00\cdot1]$ direction of the $D0_{19}$ structure. In addition, lattice fringes corresponding to the $(00\cdot2)$ plane are often observed in the amorphous region. On the basis of these data, it is concluded that a lattice destruction in the amorphous region mainly occurs in the $(00\cdot1)$ plane of the $D0_{19}$ matrix. [S0163-1829(97)07121-X]

According to a phase diagram of a Ti-Al alloy system,[1] a Ti–40 at. % Al alloy undergoes a eutectoid reaction from the α phase to the α_2 and γ phases at 1398 K. Crystal structures of the α, α_2, and γ phases are, respectively, the hcp, $D0_{19}$, and $L1_0$ structures, indicating that the reaction involves both two types of atomic ordering and a phase separation. Recently, we found an amorphous state in an initial stage of the eutectoid reaction in the Ti–40 at. % Al alloy.[2,3] Because the amorphous state is formed in the eutectoid reaction, an understanding of the state in the Ti-Al alloy is very important not only for the elucidation of the kinetics of the reaction in this alloy but also for a general understanding of the formation of an amorphous state in various materials. It should be noted that features of the crystalline to amorphous transition have so far been investigated in multilayered structures from the viewpoint of the solid state reaction and in intermetallic compounds irradiated by ion beams.[4–11]

The amorphous state in the Ti-Al alloy is formed in an intermediate stage during the structural change from the $D0_{19}$ structure to the $L1_0$ one in the eutectoid reaction.[2,3] Thus the state is associated with a reordering process accompanying a long range diffusion of solute atoms. Another important feature is that the amorphous region is nucleated in the boundary between the $D0_{19}$ matrix and the B_{19} precipitate. Note that the B_{19} precipitate is an intermediate one which subsequently disappears in the equilibrium state. These features are assumed to be crucial factors for elucidating the origin of the formation of the amorphous state in the Ti–40 at. % Al alloy. In order to obtain a better understanding of the amorphous-state formation, further characterization of the state in Ti-Al alloys is definitely needed. We have investigated both the morphological and crystallographic features of the amorphous state in the Ti–40 at. % Al alloy by transmission electron microscopy. On the basis of the experimental data, we discuss the role of crystallographic factors in the formation of the amorphous state.

An ingot of the Ti–40 at. % Al alloy was made by an Ar-arc melting technique and annealed at 1523 K for 24 h for homogenization. Samples with a size of $3\times5\times10$ mm^3 were cut from the ingot, aged at 1273 K for 15 min and quenched in ice water. Features of the amorphous state in the quenched sample were observed at room temperature using both an H-800 and an H-9000UHR transmission electron microscopes. Electron diffraction patterns, bright and dark field images, and high-resolution images were obtained in the present work. Specimens for observation were prepared by Ar-ion thinning after cutting the quenched samples into disks 30 μm in thickness and with a 1.5 mm radius. The Ar-ion thinning was carried out by using a Gatan 600-DuoMill equipped with both a rotating stage and a liquid nitrogen reservoir.

As explained in our previous papers,[2,3] the amorphous state was found to form only in the initial stage of the eutectoid reaction in the Ti–40 at. % Al alloy. In this work, we examined both the morphological and crystallographic features of the amorphous state. Figure 1 shows a series of electron diffraction patterns and corresponding dark field images, which were obtained by rotating a sample from the $[00\cdot1]_{\alpha2}$ direction to the $[11\cdot0]_{\alpha2}$ one. The suffix $\alpha2$ denotes the α_2 phase with the $D0_{19}$ structure. The electron incidences in Figs. 1(a) and 1(b) and in Figs. 1(c) and 1(d) are parallel to the $[00\cdot1]_{\alpha2}$ and the $[11\cdot0]_{\alpha2}$ directions, respectively. There is a halo ring as well as fundamental and superlattice spots in the diffraction pattern in Fig. 1(a). The fundamental and superlattice spots come from regions with the $D0_{19}$ structure, while amorphous regions give rise to the halo ring.[2,3] As for the dark field image in Fig. 1(b), which was taken by using a part of the halo ring in Fig. 1(a), there exist bandlike regions indicated by A around a stripe denoted by B in the matrix labeled as C. The most important feature is that the bandlike regions exhibit a featureless bright contrast like a liquid state. In other words, the amorphous state is formed in the bandlike region. In addition, the crystal structures of the matrix and the stripe region were analyzed to be the $D0_{19}$ and the B_{19} structures, respectively. The features shown in Fig. 1(b) are entirely consistent with those reported in our previous papers.

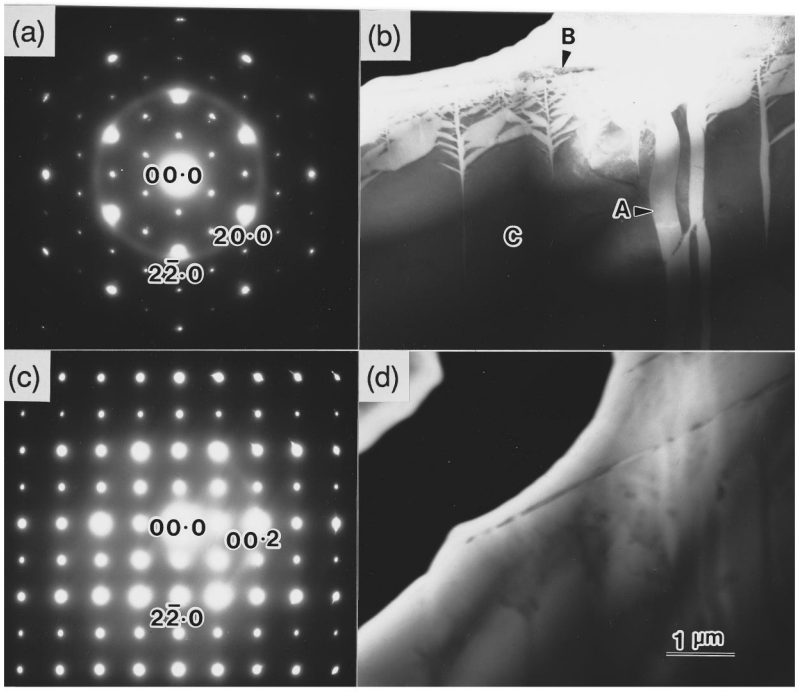

FIG. 1. Electron diffraction patterns and corresponding dark field images obtained from a sample aged at 1273 K for 15 min. Electron incidences of Figs. 1(a) and 1(b), and of Figs. 1(c) and 1(d) are parallel to the $[00\cdot1]_{\alpha2}$ and $[11\cdot0]_{\alpha2}$ directions, respectively. In the patterns, diffraction spots are indexed in terms of the $D0_{19}$ structure. Each image was taken by using a part of the first halo ring.

In order to examine the change in both the halo ring in an electron diffraction pattern and the corresponding dark field image with respect to the crystal orientation, the sample was rotated from the $[00\cdot1]_{\alpha2}$ direction to the $[11\cdot0]_{\alpha2}$ one about the $[11\cdot0]_{\alpha2}$ axis in reciprocal space. Figures 1(c) and 1(d) show the diffraction pattern and the halo dark field image in the $[11\cdot0]_{\alpha2}$ incidence, respectively. The rotation angle is 90° from the $[00\cdot1]_{\alpha2}$ direction. Although the halo ring is found in the pattern, its intensity is very weak, compared with Fig. 1(a). In Fig. 1(d), the contrast due to the amorphous state is obviously weaker than that shown in Fig. 1(b). From Figs. 1(b) and 1(d), the amorphous-state region is understood to be basically formed in the shape of a thin plate.

In order to quantitatively evaluate the intensity of the halo ring at each rotation angle, the intensity was measured by using imaging plates. Figure 2 shows the change in the intensity of the ring as a function of the rotation angle about the $[11\cdot0]_{\alpha2}$ axis. Note that the angles of 0° and 90° in Fig. 2 correspond to the $[00\cdot1]_{\alpha2}$ and the $[11\cdot0]_{\alpha2}$ electron incidences, respectively. The intensity of the ring at each angle was normalized with respect to the $11\cdot0$ superlattice spot due to the $D0_{19}$ structure. It is seen that the halo ring with the strongest intensity was obtained in the case of the $[00\cdot1]_{\alpha2}$ incidence. As the rotation angle was increased, the intensity decreased gradually and reached the weakest level in the $[11\cdot0]_{\alpha2}$ incidence.

We then examined the change in the intensity by rotating the specimen from the $[11\cdot0]_{\alpha2}$ direction to the $[10\cdot0]_{\alpha2}$ one about the $[00\cdot1]_{\alpha2}$ axis. Although the experimental data are not shown here, the measured intensities were basically weak and did not exhibit any remarkable change like that in Fig. 2. These data clearly indicate that the intensity of the halo ring shows a strong anisotropy in reciprocal space. Because the halo ring originates from the bandlike region in the dark field image, the anisotropy definitely reflects both the morphological and crystallographic features of the Ti-Al alloy. One other point should also be noted. The normal of the disk-shaped specimen is almost parallel to the $[11\cdot2]_{\alpha2}$ direction. If the formation of the amorphous state was due to Ar ion bombardment during the sample preparation, the degree of amorphization should be conspicuous in the $[11\cdot2]_{\alpha2}$ direction in Fig. 2. However, the change in the intensity is smooth and never exhibits any anomaly in the $[11\cdot2]_{\alpha2}$ direction. This is a clear indication that the amorphous state was not induced by the ion bombardment but is an essential feature in the initial stage of the eutectoid reaction in the Ti-Al alloy. In our previous work, this was also confirmed for a sample prepared by electropolishing.[2]

The anisotropy suggests a difference in crystallographic features of the amorphous state with respect to the crystallographic orientation. High-resolution transmission electron images were taken in order to examine those features. Figure 3(a) shows a high-resolution image in the $[00\cdot1]_{\alpha2}$ incidence. In the image, the letters *A* and *B* indicate the α_2 matrix and the amorphous-state region, respectively. Fringes corresponding to the $\{10\cdot0\}_{\alpha2}$ planes are seen in the α_2 matrix, while a unique contrast due to the amorphous structure is observed in almost every part of the region. An important feature of the image is that lattice fringes are present locally in the amorphous-state region, as indicated by the arrows. The size of the areas showing the lattice fringes is about 2×2 nm^2 and the spacing of the fringes corresponds to the $\{110\}_{\gamma}$ interplanar ones of the $L1_0$ structure. It is clear from this observation that the locally crystallized area present in the amorphous-state region. That is, the amorphous state in the Ti-Al alloy includes some medium-range-ordered regions, as was pointed out by Anazawa *et al.* for an amorphous state in a $Pd_{82}Si_{18}$ alloy.[12,13]

Although medium-range-ordered regions are detected, the bandlike contrast in the $[00\cdot1]_{\alpha2}$ incidence is basically due to the amorphous state. On the other hand, a dramatic change is seen in the high-resolution image in Fig. 3(b) with the electron incidence in the $[11\cdot0]_{\alpha2}$ direction. Lattice fringes

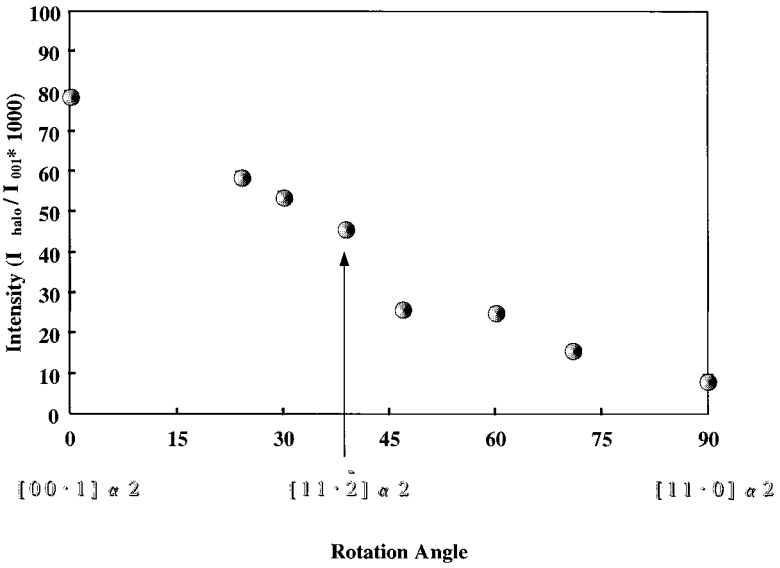

FIG. 2. Change in the intensity of the first halo ring as a function of the rotation angle of the sample. The rotation axis is parallel to the $[11\cdot0]_{\alpha2}$ direction. The intensity at each angle was normalized with respect to the $[11\cdot0]$ superlattice spot due to the $D0_{19}$ structure.

corresponding to the $(00\cdot2)_{\alpha2}$ interplanar spacing are observed over a wide area of the bandlike region, although they are not conspicuous. In other words, the lattice fringes are partially missing. According to Blackburn's relation regarding the $\alpha_2+\gamma$ lamellar structure,[14] the $(00\cdot1)_{\alpha2}$ plane is parallel to the $(111)_\gamma$ one. In addition, the $(00\cdot2)_{\alpha2}$ interplanar spacing of 0.231 nm is almost the same as that of the $(111)_\gamma$ one of 0.232 nm. This clearly implies that the period related to the spacing of the $(00\cdot2)_{\alpha2}$ plane is basically maintained in the structural change from the $D0_{19}$ structure to the $L1_0$ one. These features are obviously consistent with the fact that the lowest intensities of the halo ring were obtained in the $[11\cdot0]_{\alpha2}$ incidence, as shown in Fig.2.

The schematic diagram of the amorphous state in Fig. 4 was drawn on the basis of the above-mentioned data. The crystallographic directions of the $D0_{19}$ matrix are also shown in the diagram. The width and the thickness of the amorphous region with the plate shape were estimated to be about 0.5 μm from Fig. 1(b) and about 0.1 μm from Fig. 1(d). An interesting feature of the plate is that its tip becomes pointed, as indicated by the arrows. As for the crystallographic features, there are large areas with the $(111)_\gamma$ crystal period of the $L1_0$ structure, together with some medium-range-ordered regions inside the $(111)_\gamma$ layer. As is clear from the diagram, the amorphous state basically has a two-dimensional character with respect to both the morphological and crystallographic features.

In our previous work, the eutectoid reaction of the Ti–40 at. % Al alloy was shown to be characterized by the appearance of an amorphous region as an intermediate state. The present data indicate that the amorphous state basically has

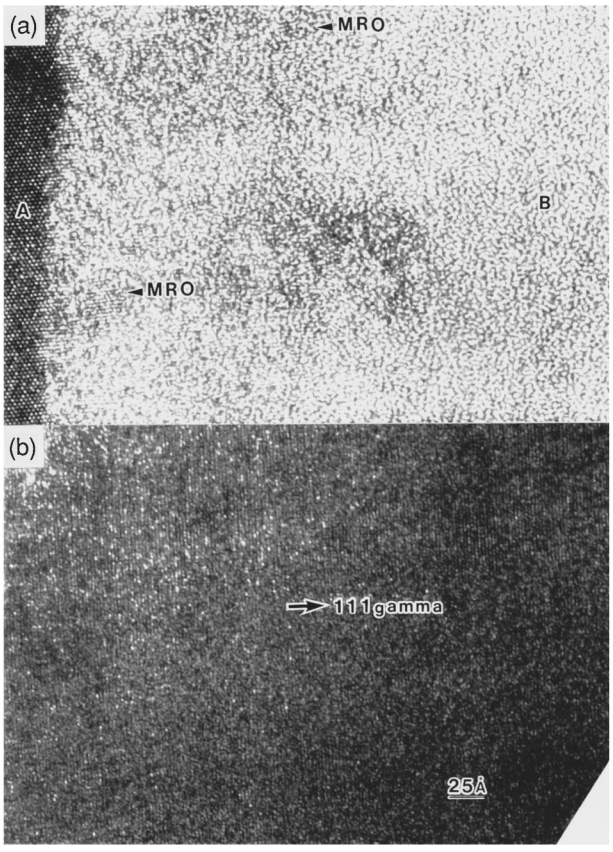

FIG. 3. High-resolution images taken from the sample aged for 15 min. Electron incidences of (a) and (b) are parallel to the $[00\cdot1]_{\alpha2}$ and $[11\cdot0]_{\alpha2}$ directions, respectively.

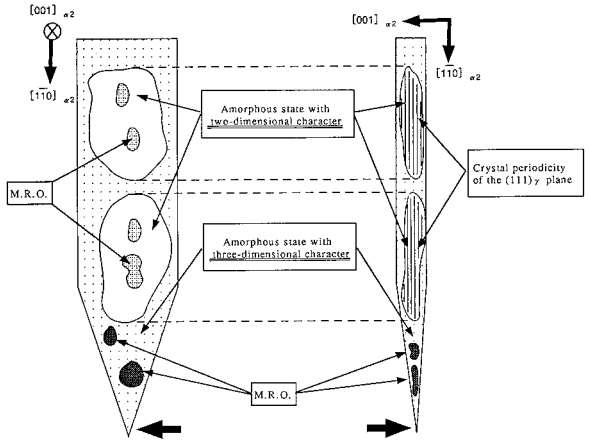

FIG. 4. Schematic diagram of an amorphous-state region appearing in the initial stage of the eutectoid reaction in the Ti–40 at. % Al alloy.

the two-dimensional character. Here we will discuss a possible reason why the amorphous state in the Ti-Al alloy has such unique features. In the eutectoid reaction, the structural change related to the appearance of the amorphous state is from the $D0_{19}$ structure to the $L1_0$ one. We then check the features of the atomic bonds involved in the $D0_{19}$ structure. As is understood from the atomic arrangement of the $D0_{19}$ structure, there are only the Ti-Ti and Ti-Al bonds in stoichiometric 25 at. % Al. On the other hand, the formation of the amorphous state has been found in the Ti–40 at. % Al alloy, which has more Al atoms than those in the stoichiometric $D0_{19}$ structure. The deviation from the stoichiometric composition would result in an increase in the numbers of the Ti-Al, Al-Al, Ti-V, and Al-V bonds, together with a decrease in that of the Ti-Ti bond, where V denotes a vacancy site. Note that experimental evidence for the generation of the vacancy states has been found in the Ti-Al alloy.[15,16] Among these bonds, Morinaga *et al.*[17] theoretically indicated that the presence of the directional Alp-Tid covalent bond causes degradation of the mechanical properties of the Ti-Al alloy. The Tid-Alp covalent bond has high bond energy. In other words, the directional Tid-Alp covalent bond can be assumed to be one of the key factors for the formation of the amorphous state in the Ti-Al alloy.

As is understood from the phase diagram,[1] the α_2 single phase with the $D0_{19}$ structure cannot exist in a composition range around 40 at. % Al as an equilibrium state. This fact clearly indicates that the quenched state with the $D0_{19}$ structure is definitely unstable and should transform to an equilibrium state. In the transition to the equilibrium state, the intermediate precipitate with the B_{19} structure appears in the $D0_{19}$ matrix. Because the B_{19} precipitate has a stoichiometric composition of 50 at. % Al, a deficiency of Al atoms would occur in the $D0_{19}$ matrix near the B_{19} precipitate. Then, there would be more Ti-V and Al-V bonds in the boundary region. The presence of these bonds would lead to displacements of the Ti and Al atoms around the vacancy from their equilibrium position. It is worth noting that the displacement is equivalent to a fluctuation of the coordination numbers for the Ti and Al atoms and presumably results in the cutting-off of the directional Tid-Alp covalent bond. In addition, because $c/a=1.604<1.633$ in the $D0_{19}$ structure, the cutting off of longer Ti-Al bonds in the $(00\cdot1)_{\alpha2}$ plane mainly occurs and leads to the two-dimensional lattice destruction. The process explained here is believed to be an appropriate origin for the two-dimensional character of the amorphous state in the Ti–40 at. % Al alloy.

Desre and Yavari showed[18,19] that during solid state amorphization of binary AB type multilayers sharp concentration gradients develop in amorphous interlayers and raise the free energy of crystalline compounds to levels near or above that of amorphous interlayers. These gradients increase the stabilization of amorphous phases against the nucleation of compounds. It seems on the basis of the present data that such gradients develop in the amorphous state of the Ti–40 at. % Al alloy. Therefore verification of the gradients is an important task for future research.

The authors would like to thank Professor M. Kikuchi and Professor M. Takeyama, Tokyo Institute of Technology, for their useful discussions concerning the subject matter of this paper.

[1] J. H. Perepezko, and J. C. Mishurda, in *Titanium '92 Science and Technology*, edited by F. H. Froes and I. Caplan (TMS, San Diego, CA, 1993), p. 563.
[2] M. Tanimura, Y. Inoue, and Y. Koyama, Phys. Rev. B **52**, 15 239 (1995).
[3] M. Tanimura, Y. Inoue, and Y. Koyama, Mater. Trans. JIM **37**, 1190 (1996).
[4] R. B. Schwarz, and W. L. Johnson, Phys. Rev. Lett. **51**, 415 (1983).
[5] R. B. Schwarz, K. L. Wong, and W. L. Johnson, J. Non-Cryst. Solids **61-62**, 129 (1984).
[6] B. M. Clemens, W. L. Johnson, and R. B. Schwarz, J. Non-Cryst. Solids **61-62**, 817 (1984).
[7] M. Van Rossum, M.-A. Nicolet, and W. L. Johnson, Phys. Rev. Lett. **29**, 5498 (1983).
[8] M. A. Hollanders, B. J. Thijsse, and E. J. Mittemeijer, Phys. Rev. B **42**, 5481 (1990).
[9] S. B. Newcomb, and K. N. Tu, Appl. Phys. Lett. **48**, 1436 (1986).
[10] Y. Limoge and A. Barbu, Phys. Rev. B **30**, 2212 (1984).
[11] P. Moine and C. Jaouen, J. Alloys Compd. **194**, 373 (1993).
[12] K. Anazawa, Y. Hirotu, and Y. Ichinose, J. Non-Cryst. Solids **156-158**, 196 (1993).
[13] K. Anazawa, Y. Hirotu, and Y. Inoue, Acta Metall. Mater. **42**, 1997 (1994).
[14] M. J. Blackburn, in *Science, Technology and Application of Titanium*, edited by R. T. Jaffee and N. E. Promisel (Pergamon, London, 1970), p. 633.
[15] G. F. Hancock and B. R. McDonnell, Phys. Status Solidi A **4**, 143 (1971).
[16] K. Maruyama, T. Takahashi, and H. Oikawa, Mater. Sci. Eng. A **153**, 433 (1992).
[17] M. Morinaga, J. Saito, N. Yukawa, and H. Adachi, Acta Metall. Mater. **38**, 25 (1990).
[18] P. J. Desre and A. R. Yavari, Phys. Rev. Lett. **64**, 1533 (1990).
[19] P. J. Desre and A. R. Yavari, J. Alloys Compd. **194**, 229 (1993).